Available online at www.sciencedirect.com
ScienceDirect
International Journal of Heat and Mass Transfer 51 (2008) 1453–1466
International Journal of HEAT and MASS TRANSFER
www.elsevier.com/locate/ijhmt

Prediction of enthalpy production from fractured geothermal reservoirs using partitioning tracers

Xingru Wu [a,*], Gary A. Pope [b], G. Michael Shook [c], Sanjay Srinivasan [b]

[a] BP America Inc., 501 Westlake Park Blvd, Houston, TX 77079, USA
[b] The University of Texas at Austin, Austin, TX 78712, USA
[c] Chevron Energy Technology Company, Houston, TX 77002, USA

Received 22 January 2007
Available online 20 August 2007

Abstract

The goal of geothermal reservoir management is to economically recover as much energy as possible from the reservoir. This paper presents the development of improved techniques for monitoring and predicting two-phase mass and heat transport in fractures. Partitioning tracers can yield valuable, early information about fracture properties used within a semi-analytical approach for calculating enthalpy production from the fractured system. This is demonstrated for a synthetic model with a fracture network. The comparisons of the semi-analytical solutions with the simulation results show that the model predicts enthalpy production is easy, fast and ideally suited for sensitivity studies.
Published by Elsevier Ltd.

Keywords: Flow in fractures; Geothermal; Partitioning tracers; Enthalpy production

1. Introduction

Re-injection of spent geothermal fluids is a preferred reservoir management strategy to increase energy extraction efficiency and maintain reservoir pressure that is being practiced in many geothermal reservoir fields such as the Geysers, California [1]. However, without careful reservoir characterization and an understanding of reservoir properties that affects heat transfer, cold water injection could lead to premature breakthrough and defeat the goal of enhancing energy extraction efficiency.

Geothermal tracer testing is a very powerful tool for the characterization and management of geothermal reservoirs. When a partitioning tracer is injected into a superheated geothermal reservoir, tracer transport occurs in the vapor phase resulting in a faster chemical breakthrough than thermal breakthrough [2,3]. The tracer test can therefore provide early information on important interwell flow properties that can be used to optimize injection well location and manage energy extraction. However, geothermal tracer test analysis currently performed provides solely a qualitative assessment of reservoir property variations. Therefore, it is imperative to develop techniques that would yield a more quantitative assessment of key reservoir properties, especially in the case of fractured reservoirs. Reliable prediction of enthalpy production and thermal recovery efficiency in fractured geothermal reservoirs can then be obtained.

Several authors [4–6] have shown analytical solution of temperature in a fracture corresponding to single-phase liquid flow in the fracture with heat conduction from a semi-infinite matrix, and the solution is also given in Carslaw and Jaeger [7]. Bodvarsson and Tsang [8] studied a finite matrix model with assumptions of single liquid phase radial flow in horizontal fractures. Temperature profiles corresponding to several boundary and initial conditions were calculated with an aim to design the locations of injection wells and the injection rate. Assumptions such as single liquid phase flow and infinite matrix size were made to

* Corresponding author. Tel.: +1 281 366 0003; fax: +1 281 366 5717.
E-mail addresses: Xingru.Wu@bp.com, wuxru@yahoo.com (X. Wu).

0017-9310/$ - see front matter Published by Elsevier Ltd.
doi:10.1016/j.ijheatmasstransfer.2007.06.023

Nomenclature

A	cross section area normal to flow direction
b	half fracture aperture
C	tracer concentration
C_p	specific heat capacity
D	half fracture spacing
f_i	flow capacity of individual streamline
F	flow capacity of a porous media
H	distance between the producer and the injector
$\underline{H}$	enthalpy of fluid per unit mass
$\dot{H}_{\mathrm{P}}$	enthalpy production rate
H_{P}	cumulative enthalpy production
k	permeability of media
K_i	equilibrium distribution coefficient of component i
L	fracture length normal to the flow direction
L_{V}	latent heat of water at certain temperature
m	mass of tracer recovered at the producers
$\dot{m}$	mass flow rate
M	total mass of injected tracer
M_{R}	mass flow ratio
$M_{\mathrm{T}j}$	overall volumetric thermal capacity of fracture with phase j
P	pressure
q_{inj}	volumetric injection rate of liquid water
R	thermal recovery efficiency
R_i	flow/storage ratio of ith streamline
s	Laplace variable
T	temperature
t	time
t^*	mean residence time
u	superficial velocity
V	cumulative production volume of vapor phase
$\bar{V}$	mean residence volume
V_{DT}	velocity retardation factor because of liquid vaporization at the boiling interface
V_{p}	swept pore volume
V_{s}	cumulative production volume of vapor phase during the time of tracer injection
v	interstitial velocity
x_i	mole fraction of species i in aqueous phase
y_i	mole fraction of species i in vapor phase

Greek symbols

α	thermal diffusivity
λ	thermal conductivity of rock matrix
φ_i	storage capacity of individual streamline
Φ	storage capacity of a porous media
ρ	density
ϕ	porosity of the reservoir
ϑ	dimensionless variable
ψ	dimensionless variable
υ	dimensionless temperature in the matrix in Laplace space
η	dimensionless temperature in the fracture in Laplace space
$\Re$	thermal recovery efficiency in Laplace space

Subscripts

D	denotation of dimensionless variable
I	initial condition
J	injection condition
f	fracture property or front
m	matrix property
r	rock
v	vapor phase water
w	liquid phase water

obtain the solutions and these assumptions might not hold for typical geothermal reservoirs.

When cold liquid water is injected into superheated geothermal reservoirs, the injected liquid phase will boil and transport as steam toward the producers. Thus, the assumption of single-phase flow is not appropriate and leads to inaccurate predictions. In addition, most naturally fractured reservoirs have finite fracture spacing and hence the assumption of semi-infinite matrix blocks is also invalid. The goal of this research is to develop a fast and more accurate model to calculate enthalpy production and thermal recovery efficiency with realistic fracture spacing and under two-phase flow conditions.

Based on a conceptual fracture model description and assumptions, we present a new semi-analytic solution for enthalpy production (or, more generally, temperature as a function of time and spatial dimensions x and z) in a single fracture model, in which the assumptions of semi-infinite block size are relaxed. This solution is later expanded to the two-phase flow scenario in a network of multiple fractures. We identify the reservoir parameters that must be known to implement the semi-analytic solution, and propose the use of tracer analysis to estimate those properties. This approach is demonstrated for the case of a fracture network. Numerical simulation is used as a tool to validate the semi-analytic solution on some synthetic cases.

2. Conceptual geothermal model

Geothermal reservoirs are usually very complex, fractured reservoirs containing multiple fluid phases and complex phase transitions, chemical reactions, and energy transport via both conduction and convection. In naturally fractured geothermal reservoirs, the rock matrix stores most of energy, while the fracture networks serve as flow conduits. The matrix often has very low permeability, typically of the order of 10^{-18} m^2 or less [9] while the perme-

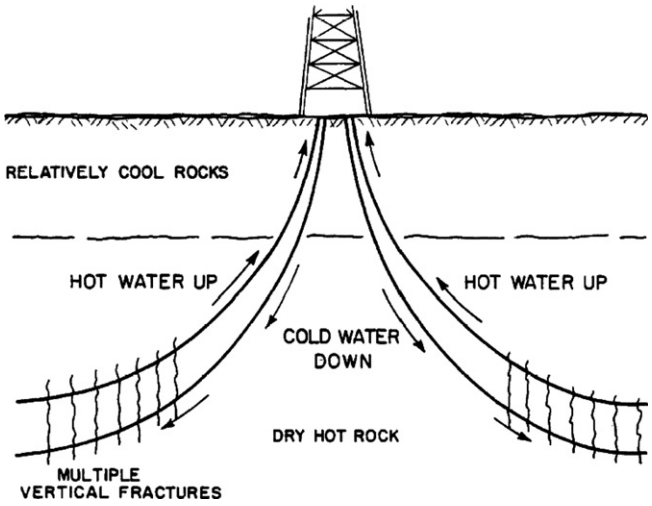

Fig. 1. Schematic diagram of vertical fractures in geothermal reservoirs (after Gringarten et al. [10]).

ability of a fracture with aperture of 10^{-4} m could be as high as in the order of 10^{-10} m^2 the permeability contrast between fracture and matrix is therefore very high. The fracture permeability can be empirically correlated to fracture aperture and porosity of the fracture in literature [10]; however, in the following discussion and examples it is treated as a constant quantity. A conceptual model for a geothermal reservoir in which the vertical fractures dominate is shown in Fig. 1. In this diagram, an injector and a producer penetrates a series of parallel vertical fractures separated by impermeable matrix blocks. The producer is completed in the upper part of the reservoir and the injector is completed in the lower part of the reservoir so as to promote gravity-stable flow.

This conceptual model can be simplified somewhat to permit a detailed analysis. Initially, a single fracture was explicitly modeled so that the transient processes of heat and mass transfer could easily be visualized, as shown in Fig. 2. Due to symmetry, only one half plane of the fracture and matrix block were modeled as shown in Fig. 3. Because it is a symmetry element, the boundary of the matrix was set to no heat-flow condition as shown in Fig. 3. An injection point (injector) is located at the bottom of the fracture and an extraction point (producer) is at the other end of the fracture. Initially the geothermal reservoir is in thermodynamic equilibrium and temperature distribution is homogeneous in the model.

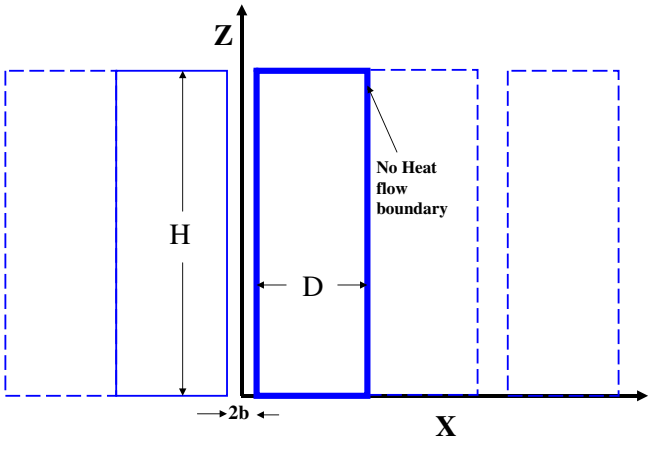

Fig. 2. Diagram of a symmetric element from equal spaced fracture network.

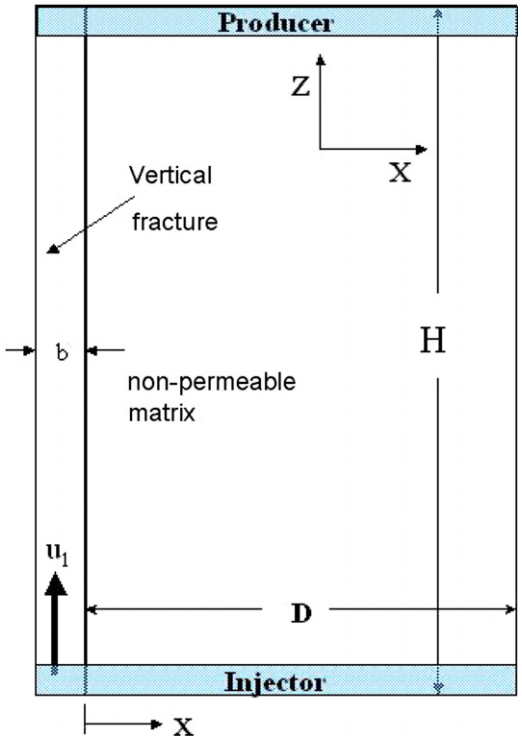

Fig. 3. Diagram of a single fracture model that is used to model a fracture network with equally spaced, parallel vertical fractures.

In reality geothermal reservoirs are likely to have a network of fractures rather than a single fracture. It is also very likely that the network is characterized by a range of fracture aperture, porosity, permeability, and fracture spacing, even if the fractures are all assumed to be vertical. Fig. 4 shows a diagram of an idealized fracture network with vertical fractures and varying properties for the fractures. The objective of this research is to estimate the enthalpy production from a fracture network in geothermal reservoir; this model is a simplified representation of such a network. The solutions we develop below are valid (if approximate) for fractured reservoirs whose fractures trend in a single direction and under conditions of stable displacement (i.e., no bypassing by the injected fluids). Variations in fracture spacing or aperture can be accommodated as long as those variations occur at scales small relative to the bulk property. For example, a dogleg in a fracture is unimportant as long as the *relative* change in fracture spacing is small. One can imagine similar violations of the underlying assumptions such as large variations in thermal properties of the rock matrix. These and

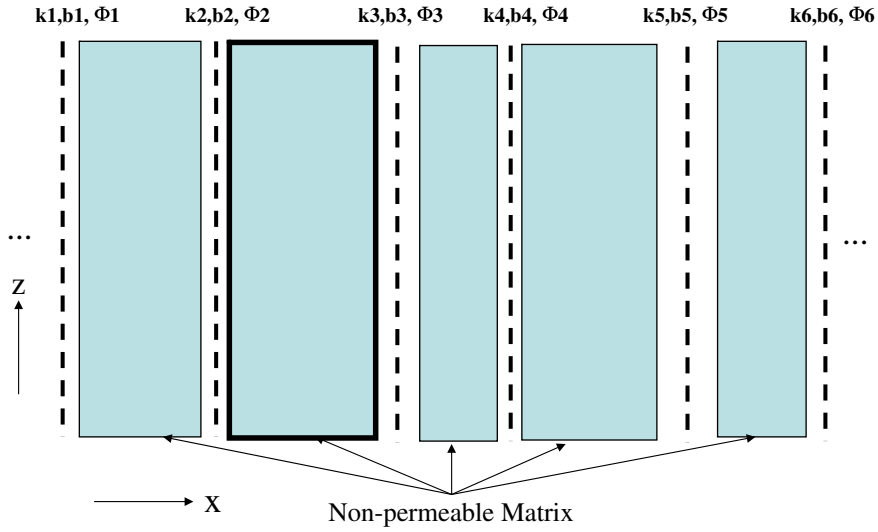

Fig. 4. Discrete fracture network with varying fracture properties.

other conditions where heat conduction in multiple dimensions is important (e.g., reservoirs with multiple sets of fractures) are beyond the scope of this work.

In this paper, we develop semi-analytical solutions to estimate enthalpy production and thermal recovery based upon energy balance analysis from our simplified fractured geothermal reservoir. The semi-analytic solution requires knowledge of reservoir properties as input. We propose tracer interpretation as a means of estimating the required properties. Some fundamental theory about tracer test analysis and estimation of required parameters are shown below.

3. Tracer test analysis

Estimation of enthalpy production and recovery from geothermal reservoirs requires knowledge of the following parameters for both the single fracture and fracture network models discussed here.

(1) Thermal properties (heat capacity and conductivity) of reservoir rock.
(2) Thermodynamic properties of fluids, both in situ and injected.
(3) Fracture properties such as permeability, porosity, aperture, and heat transfer area.
(4) Interstitial velocities of fluids in the fracture or fracture network.
(5) Matrix dimensions and properties such as porosity of the impermeable rock (only necessary to determine the effective heat capacity of the matrix).

Parameters such as the thermal properties of rock and thermodynamic properties of fluids are available in literature and are assumed known for the results presented in this paper. However, parameters such as fracture properties and interstitial velocities are reservoir specific and unknown a priori. It is demonstrated below that these parameters can be estimated from tracer testing.

Tracer selection for a specific geothermal reservoir requires careful assessment of the positive and negative features of potential tracer candidates. The optimal tracer should not only satisfy all the requirements for a successful tracer test, but also pass stringent environmental requirements. Wu et al. [11] showed that for superheated geothermal reservoirs, highly volatile tracers should be used in order to obtain early information about reservoir properties and fluid flow velocity. The volatility of the tracer is represented by the equilibrium coefficient (K). In this paper, a representative K value of 4500 is used under the superheated geothermal reservoir conditions. The estimation of K values under geothermal reservoir condition is shown in the paper. A typical tracer return curve is shown in Fig. 5. This figure shows tracer concentration history in the vapor phase at a superheated reservoir and it shows that the tracer information can give reservoir information within a very short time – on the order of couples of months.

3.1. Method of moments

The analysis uses the first temporal moment of the tracer concentration history (sometimes known as a breakthrough curve) recorded at the producer to calculate the pore volume contacted by the injected tracer (the swept pore volume). This method has a rigorous theoretical basis and has been widely used in both groundwater and oil field applications [12,13]. It can be used in the absence of detailed reservoir characterization data or flow and transport models, since only a very simple, fast and easy integration of the tracer production data is needed to yield the mean residence time. The first moment with respect to produced fluid volume from a finite tracer slug is defined as [14,15]:

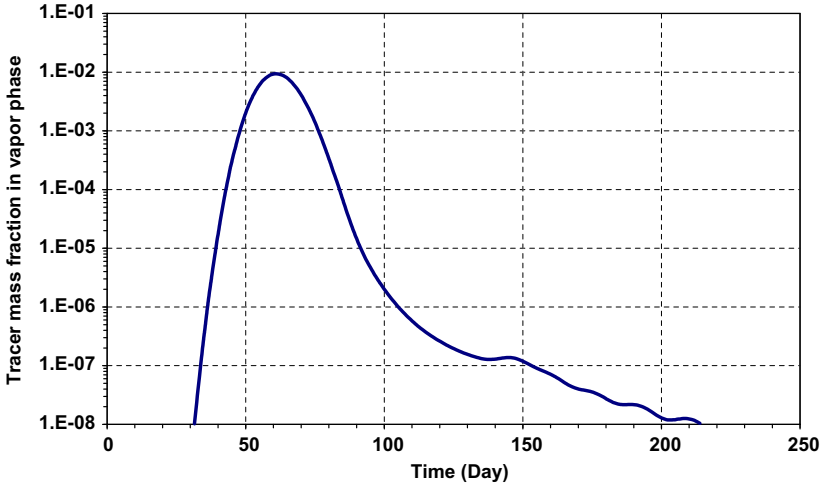

Fig. 5. A typical tracer curve in a superheated geothermal reservoir.

$$\overline{V} = \frac{\int_0^\infty VC(t)\,\mathrm{d}V}{\int_0^\infty C(t)\,\mathrm{d}V} - \frac{V_s}{2} \tag{1}$$

where V_s is the volume of fluid produced during tracer injection.

The calculated volume from Eq. (1) is the total pore volume swept by the tracer under the assumption that the tracer flows simultaneously with the carrier fluids. To apply the method of moments for geothermal application, we make following assumptions (1) tracer is injected with liquid phase, (2) tracer with a high K value will partition into the vapor phase immediately in the phase transition process. Wu et al. [11] showed that the estimation of swept fracture pore volume from highly volatile tracer is very accurate for superheated reservoirs with impermeable rock matrix. By using the method of moments, the swept fracture pore volume for the complete fracture network is determined easily.

3.2. Fluid velocities in fracture network

Fluid velocities are also required to estimate enthalpy production and thermal recovery. These are obtainable from a Flow Capacity/Storage Capacity diagram. The flow capacity and storage capacity were originally used to quantify the heterogeneity of a layered model in porous media [16]. They were generalized to include arbitrary flowpath lengths by Shook [17]. The volumetric flow capacity, f_i, of a streamline follows directly from Darcy's law; a given streamline's flow capacity is proportional to its permeability and cross sectional area, and inversely proportional to its length. The storage capacity, φ_i, of that streamline is simply its pore volume. By defining a ratio of flow-to-storage, $R_i = f_i/\varphi_i$, and ranking all streamlines in descending order of R, the cumulative flow capacity at any given streamline "i" is given as the sum of all streamlines with $R > R_i$. The cumulative storage capacity is the sum of those streamlines' pore volume. Both are normalized by the ensemble property:

$$F_i = \frac{\sum_{j=1}^{i} k_j A_j / L_j}{\sum_{j=1}^{N} k_j A_j / L_j} \quad (2a)$$

$$\Phi_i = \frac{\sum_{j=1}^{i} k_j A_j L_j}{\sum_{j=1}^{N} k_j A_j L_j} \quad (2b) \tag{2}$$

For the case of uniform flowpath lengths these definitions collapse to the classic definitions found in the literature [16]

$$F_i = \frac{\sum_{j=1}^{i} k_j h_j}{\sum_{j=1}^{N} k_j h_j} \quad (3a)$$

$$\Phi_i = \frac{\sum_{j=1}^{i} \phi_j h_j}{\sum_{j=1}^{N} \phi_j h_j} \quad (3b) \tag{3}$$

Flow capacity, F, and storage capacity, Φ, are most frequently plotted on an F–Φ (or Lorentz) diagram. An important feature of F–Φ curves is that, under certain conditions, interstitial velocities of individual fractures can be determined directly.

Shook [17] shows that flow capacity, F, can be determined from the zeroth moment and the storage capacity, Φ, in terms of the first order moment of the tracer history:

$$F = \frac{\int_0^t C\,\mathrm{d}t}{\int_0^\infty C\,\mathrm{d}t} \quad (4a)$$

$$\Phi = \frac{\int_0^t Ct\,\mathrm{d}t}{\int_0^\infty Ct\,\mathrm{d}t} \quad (4b) \tag{4}$$

The derivative of F with respect to Φ is a ratio of the mean residence time divided by the residence time of the ith fracture. If we assume equal length flow paths (as we have done in our conceptual model), this ratio becomes a ratio of velocities: the interstitial velocity of the ith fracture normalized by the mean velocity of the network

$$\frac{\partial F}{\partial \Phi} = \frac{\frac{\partial F}{\partial t}}{\frac{\partial \Phi}{\partial t}} = \frac{\frac{C}{\int_0^\infty C\,\mathrm{d}t}}{\frac{Ct}{\int_0^\infty Ct\,\mathrm{d}t}} = \frac{1}{t}\frac{\int_0^\infty Ct\,\mathrm{d}t}{\int_0^\infty C\,\mathrm{d}t} = \frac{t^*}{t_i} = \frac{v_i}{\overline{v}}\frac{\overline{L}}{L_i} \tag{5}$$

For a fracture network, a plot of $\frac{\partial F}{\partial \Phi}$ vs. Φ yields valuable information about the variation in interstitial velocities in the heterogeneous reservoir. An example of such a plot is shown in Fig. 9, in which there are two fractures (arbitrarily named 1 and 2 in the figure). The number of fractures and their fractional pore volume are identified from the inflextion points on the curve. In this case, Fracture 1 comprises approximately 33% of the total pore volume, and has a relative velocity of 1.5 times the average (the average value for fracture 1). Fracture 2 holds 67% of the pore volume and has a relative velocity of 0.75.

Supposing a system has two major fractures as in Fig. 9, then the ratio of mass flow rates through the individual fractures is given by:

$$M_{\mathrm{R}} = \frac{\dot{m}_1}{\dot{m}_2} = \frac{v_1 \phi_{\mathrm{f1}} b_1 L_1 \rho H}{v_2 \phi_{\mathrm{f2}} b_2 L_2 \rho H} = \frac{v_1 V_{\mathrm{p1}}}{v_2 V_{\mathrm{p2}}} \tag{6}$$

For cases where $\frac{\partial F}{\partial \Phi}$ is a ratio of velocities (i.e., equal flowpath lengths), the mass flow rate ratio is the product of the ratio of interstitial velocities and the ratio of pore volumes of the fractures. The total injection mass rate is usually known, so the mass flow rate through each individual fracture can be calculated from Eq. (6). In case of multiple fractures, multiple velocity ratios and pore volume ratios can be calculated by following the same methodology.

3.3. Velocity of boiling interface

To estimate the enthalpy production and thermal recovery for superheated geothermal reservoirs, the steam flow rate and liquid front moving velocity need to be quantitatively determined with consideration of phase transition. Since fluid flow occurs only in the fracture in our model, the relationship between the two velocities along the fracture can be derived by analyzing the mass and energy balances. The following assumptions are made:

- Heat conduction neglected in the flow direction.
- Local thermodynamic and hydrodynamic equilibrium.
- The liquid and steam have a sharp front, and vaporization occurs only at the front. The temperature ahead of the front is the initial reservoir temperature, T_{I}. The temperature at the front is an interface temperature T_{i}, the value of which is dictated by reservoir pressure.
- Compressibility of rock and liquid neglected.
- Variations in liquid and steam densities from initial reservoir temperature (240 °C) to the boiling temperature at the interface are small under geothermal conditions, and can be neglected. Variations in liquid density are small because of its low compressibility. Steam density variations are small because the pressure gradient within the steam zone are small, and the steam phase only exists between the initial reservoir temperature and the interfacial temperature, which is typically a small value.

Denoting the liquid flow rate in the fracture as v_J, and steam flow rate as v_p. The diagram of this one-dimensional flow is illustrated in Fig. 7. At time t_1, the liquid front is assumed to be located at x_1. After a duration Δt, the position of the front should be x_2 assuming no vaporization. However, because of vaporization, the actual location of the front would be at x_{f} at that time, $t_2 = t_1 + \Delta t$.

The mass balance equation over a control volume of size Δx is:

$$\rho_{\mathrm{w}} A \Delta x \phi - \rho_{\mathrm{v}} A \Delta x \phi = A \phi v_{\mathrm{J}} \rho_{\mathrm{w}} \Delta t - A \phi v_{\mathrm{p}} \rho_V \Delta t \tag{7}$$

Eq. (7) can be solved for the liquid front velocity, v_{f}:

$$v_{\mathrm{f}} = \frac{\Delta x}{\Delta t} = \frac{v_{\mathrm{J}} \rho_{\mathrm{w}} - v_{\mathrm{p}} \rho_{\mathrm{v}}}{\rho_{\mathrm{w}} - \rho_{\mathrm{v}}} \tag{8}$$

The energy balance over the same control volume yields:

$$A \Delta x (1-\phi) \rho_{\mathrm{r}} C_{pr} (T_{\mathrm{I}} - T_{\mathrm{i}}) = A \phi [x_2 - (x_1 + \Delta x)] \rho_{\mathrm{w}} L_{\mathrm{v}} \tag{9}$$

where T_{I} is the initial reservoir temperature, and T_{i} is the boiling temperature at the interface. Dividing by Δt:

$$\frac{\Delta x}{\Delta t}(1-\phi) \rho_{\mathrm{r}} C_{pr} (T_{\mathrm{I}} - T_{\mathrm{i}}) = \left[\frac{x_2 - x_1}{\Delta t} - \frac{\Delta x}{\Delta t} \right] \rho_{\mathrm{w}} \phi L_{\mathrm{v}} \tag{10}$$

Rearranging Eq. (10), the relationship between the liquid injection velocity $\left(\frac{x_2 - x_1}{\Delta t}\right)$ and liquid front velocity $\left(\frac{\Delta x}{\Delta t}\right)$ is:

$$\frac{v_{\mathrm{f}}}{v_{\mathrm{J}}} = \frac{\rho_{\mathrm{w}} L_{\mathrm{v}}}{\rho_{\mathrm{w}} L_{\mathrm{v}} + \frac{(1-\phi)}{\phi} \rho_{\mathrm{r}} C_{pr} (T_{\mathrm{I}} - T_{\mathrm{i}})} \tag{11}$$

Define:

$$V_{\mathrm{DT}} = \frac{(1-\phi)}{\phi} \frac{\rho_{\mathrm{r}} C_{pr} (T_{\mathrm{I}} - T_{\mathrm{i}})}{\rho_{\mathrm{w}} L_{\mathrm{v}}} \tag{12}$$

Here V_{DT} is the velocity reduction factor caused by liquid vaporization at the interface. Eq. (11) can be written as:

$$\frac{v_{\mathrm{f}}}{v_{\mathrm{J}}} = \frac{1}{1 + V_{\mathrm{DT}}} \tag{13}$$

The velocity retardation factor, V_{DT}, generally has a finite value greater than zero and so the right hand side is less than 1, implying that the front velocity is slower than the injection velocity. Solving Eqs. (8) and (13) gives the vapor phase production rate

$$v_{\mathrm{p}} = \frac{v_{\mathrm{J}} (\rho_{\mathrm{w}} V_{\mathrm{DT}} + \rho_{\mathrm{v}})}{\rho_{\mathrm{v}} (1 + V_{\mathrm{DT}})} \tag{14}$$

Although Eqs. (8) and (13) are derived for flow in a one-dimensional porous media, they can be applied to fractured reservoirs with impermeable matrix. This is because, the thermal breakthrough occurs fairly early in the life of a typical geothermal reservoir, and heat transferred from the matrix is limited to that time. Additionally, the temperature gradient between the matrix and the fracture in the vapor zone is low so that heat flux is minimal at early times.

With the assumption that the flowing steam and liquid are separated by a sharp front in between, the whole reservoir is divided into two zones and the enthalpy and temperature distribution in each zone is solved separately as shown in following discussion.

4. Mathematical formulation of energy production for single fracture reservoir

We first derive a solution for enthalpy production for liquid injection into an initially superheated single fracture with an adjacent finite width rock matrix (see Fig. 3). This is subsequently extended to a fracture network. The following key assumptions have been made:

(1) Heat conduction in the matrix parallel to flow is negligible. Because flow in the fracture is much faster than heat conduction in the matrix, heat conduction can be treated in one dimension.
(2) Thermal properties of rock and liquid are constant.
(3) Heat conduction in the fracture is neglected.
(4) Uniform initial temperature.
(5) Constant injection rate and temperature.
(6) Local thermodynamic equilibrium.
(7) Fluid density and viscosity of the steam and liquid are constant under reservoir conditions.
(8) Liquid is injected, some of which boils with a sharp interface between regions of liquid flow and vapor flow.

We denote subscript $j = \mathrm{w}$ as liquid flow region and $j = \mathrm{v}$ as the vapor flow region in following mathematical derivation of the solution.

The heat transfer in the matrix is only by conduction and hence the energy balance in the matrix in each region is given by:

$$\frac{\partial T_{\mathrm{m}j}}{\partial t} = \frac{\lambda}{\rho_{\mathrm{r}} C_{\mathrm{r}}} \frac{\partial^2 T_{\mathrm{m}j}}{\partial x^2} \tag{15}$$

The heat conduction in the matrix in z-direction is neglected because of small temperature gradient in this direction as the fluid flow is in the x-direction.

The heat transfer in the fracture is by convection of the fluid in the fracture and conduction of heat from the matrix:

$$M_{\mathrm{T}j} \frac{\partial T}{\partial t} + \rho_j \vec{u}_j C_{pj} \frac{\partial T}{\partial z} - \frac{\lambda}{b} \frac{\partial T_{\mathrm{r}}}{\partial x}\bigg|_{x=0} = 0$$
$$j = \text{liquid water or steam in different zones} \tag{16}$$

In Eq. (16), we defined $M_{\mathrm{T}j}$, the volumetric heat capacity of rock saturated with fluid j, and it can be calculated as:

$$M_{\mathrm{T}j} = \phi \rho_j C_{pj} + (1-\phi)\rho_{\mathrm{r}} C_{p\mathrm{r}}$$

The initial and boundary conditions are:

$$T_{\mathrm{f}}(x,0) = T_{\mathrm{m}}(x,z,0) = T_{\mathrm{I}}$$
$$T(0,t) = T_{\mathrm{J}}$$
$$T_{\mathrm{f}}(z,t) = T_{\mathrm{m}}(0,z,t)$$
$$\frac{\partial T_{\mathrm{m}}}{\partial x}\bigg|_{x=D} = 0$$

where T_{I} and T_{J} are the initial reservoir temperature and the injection temperature, respectively; T_{f} and T_{m} are the temperatures in the fracture and matrix, respectively. Defining the following dimensionless variables:

$$T_{\mathrm{D}} = \frac{T - T_{\mathrm{I}}}{T_{\mathrm{J}} - T_{\mathrm{I}}}; \quad X_{\mathrm{D}} = \frac{x}{D}; \quad Z_{\mathrm{D}} = \frac{z}{H}$$
$$t_{\mathrm{D}j} = \frac{q_{\mathrm{inj}}}{V_{\mathrm{pfr}}(1 + D_{\mathrm{T}j})} t$$
$$\vartheta_j = \frac{\alpha_{\mathrm{r}}}{D^2} \frac{V_{\mathrm{pfr}}(\mathbf{1} + D_{\mathrm{T}j})}{q_{\mathrm{inj}}}$$
$$\psi_j = \frac{\lambda}{M_{\mathrm{T}j} b D} \frac{V_{\mathrm{pfr}}(\mathbf{1} + D_{\mathrm{T}j})}{q_{\mathrm{inj}}}$$

Physically, V_{pfr} is swept pore volume in the fractures estimated from Eq. (2), and the dimensionless time t_{D} is liquid injection time normalized by the thermal breakthrough time at the producer. $D_{\mathrm{T}j}$ is the thermal retardation factor for liquid water or steam given by:

$$D_{\mathrm{T}j} = \frac{(\mathbf{1} - \phi_{\mathrm{f}})\rho_{\mathrm{r}} C_{p\mathrm{r}}}{\phi_{\mathrm{f}} \rho_j C_{pj}}$$

The thermal retardation factor, D_{T}, reflects the difference between the fluid moving velocity and thermal front velocity in porous media. The two velocities are different because thermal energy travels through both fluid-filled pores and the rock fabric [3]. It is also different with the velocity retardation factor mention previously since the latter factor is caused by liquid vaporization at the boiling front.

Recasting Eqs. (15) and (16) and the initial and boundary conditions using the dimensionless variables:

$$\frac{\partial T_{\mathrm{D}mj}}{\partial t_{\mathrm{D}j}} = \vartheta \frac{\partial 2 T_{\mathrm{D}mj}}{\partial X_{\mathrm{D}}^2} \tag{17}$$
$$\frac{\partial T_{\mathrm{D}j}}{\partial t_{\mathrm{D}j}} + \frac{\partial T_{\mathrm{D}j}}{\partial Z_{\mathrm{D}}} - \psi \frac{\partial T_{\mathrm{D}mj}}{\partial X_{\mathrm{D}}}\bigg|_{X_{\mathrm{D}}=0} = \mathbf{0} \tag{18}$$

and the initial and boundary conditions are:

$$T_{\mathrm{D}j}(X_{\mathrm{D}}, 0) = T_{\mathrm{D}r}(X_{\mathrm{D}}, Z_{\mathrm{D}}, 0) = 0$$
$$T_{\mathrm{f}}(0, t_{\mathrm{D}}) = 1 \quad \text{for } t_{\mathrm{D}} \geqslant 0$$
$$T_{\mathrm{D}j}(Z_{\mathrm{D}}, t_{\mathrm{D}j}) = T_{\mathrm{D}r}(Z_{\mathrm{D}}, 0, t_{\mathrm{D}j})$$
$$\frac{\partial T_{\mathrm{D}r}}{\partial X_{\mathrm{D}}}\bigg|_{X_{\mathrm{D}}=1} = 0$$

Eqs. (17) and (18) with the boundary and initial conditions are solved using Laplace transform in Appendix A. The temperature of the liquid phase region in the fracture in terms of Laplace variables s is:

$$\eta = \frac{f(z_{\mathrm{D}})}{s} \tag{19}$$

and in the matrix:

$$\upsilon = \frac{f(z_D)}{s}\left[\cosh\left(\sqrt{\frac{s}{\vartheta_w}}X_D\right) - \sinh\left(\sqrt{\frac{s}{\vartheta_w}}X_D\right)\tanh\left(\sqrt{\frac{s}{\vartheta_w}}\right)\right] \tag{20}$$

where

$$f(z_D) = \exp\left[-\left(\psi_w\sqrt{\frac{s}{\vartheta_w}}\tanh\left(\sqrt{\frac{s}{\vartheta_w}}\right) + s\right)z_D\right] \tag{21}$$

For the vapor phase, the boundary condition at the interface is the interface temperature, T_i, which is induced by the extraction pressure. Defining the dimensionless interface temperature as ϖ:

$$\varpi = \frac{T_i - T_I}{T_J - T_I}$$

Following a procedure similar to the one used in the derivation of the liquid flow equation, we get the following Laplace solution for dimensionless temperatures:

$$u_v = \frac{\varpi}{s}f(z_D) \tag{22}$$

in the fracture, and in the matrix

$$v_v = \frac{\varpi}{s}f(z_D)\left[\cosh\left(\sqrt{\frac{s}{\vartheta_v}}X_D\right) - \sinh\left(\sqrt{\frac{s}{\vartheta_v}}X_D\right)\tanh\left(\sqrt{\frac{s}{\vartheta_v}}\right)\right] \tag{23}$$

Specially when $\varpi = 0$ then $T_i = T_I$ i.e. there is no temperature drop at the liquid/vapor interface, the dimensionless temperature in Laplace space is zero and the solution is trivial.

4.1. Enthalpy production and thermal recovery

For superheated geothermal reservoir, the temperature history can be temporally divided into several periods. At first there is a period of steam production followed by liquid production at boiling temperature, and then the temperature of working fluid decline gradually. With assumptions made in previous sections, once the fluid temperature is known, the enthalpy production rate corresponding to the two-phase flow can be calculated from following equation:

$$\dot{H}_p = \dot{m}_w C_{pw} T_w + \dot{m}_v \underline{H}_v \tag{24}$$

H_V is vapor phase enthalpy and the cumulative energy production is

$$H_p = \int_0^{t_s} \dot{m}_v \underline{H}_v \,dt + \int_{t_s}^{t} \dot{m}_w C_{pw} T_w \,dt \tag{25}$$

where t_s is the time of vapor production. The sharp interface front moves along the fracture till breakthrough at the producer at t_s.

4.2. Special case – single-phase liquid initial condition

If initially only liquid phase present in the reservoir, the solution for this special case is identical to Eqs. (19) and (20). From the Appendix, when $D \to 0$, the dimensionless temperature in dimensionless time space is:

$$T_{fD} = \delta(t_D - Z_D) \tag{26}$$

where $\delta(t_D - Z_D)$ is a Dirac's Delta Function with following property:

$$\delta(t_D - Z_D) = \begin{cases} 1 & t_D \geqslant Z_D \\ 0 & t_D < Z_D \end{cases} \tag{27}$$

In other words, in one-dimensional flow, the temperature profile is in the form of a sharp front that changes from the injection temperature to the initial temperature.

When $D \to \infty$, in dimensionless time space, the dimensionless temperature corresponding to the single-phase system is as follows:

$$T_{fD} = \operatorname{erfc}\left\{\frac{\psi Z_D}{2[\vartheta(t_D - Z_D)]^{1/2}}\right\} \tag{28}$$

In this situation, the matrix block is infinite and Eq. (28) is identical with the solution in Carslaw and Jaeger [7].

4.2.1. Enthalpy production for single-phase liquid

The dimensionless temperature of liquid phase water at the producer (where $z = H$ so that $z_D = 1$) can be calculated from Eqs. (19) and (21):

$$\eta = \frac{1}{s}\exp\left[-\left(\psi_w\sqrt{\frac{s}{\vartheta_w}}\tanh\left(\sqrt{\frac{s}{\vartheta_w}}\right) + s\right)\right] \tag{29}$$

When the temperature is known, the enthalpy production rate is as follows.

$$\dot{H}_P = \dot{m}_w C_{pw} T_w \tag{30}$$

and the cumulative energy production is calculated as

$$H_p = \int_0^{t'} \dot{m}_w C_{pw} T_w \,dt \tag{31}$$

Assuming that the density and thermal capacity of the work fluid are independent of time, solving Eq. (31) in Laplace space gives:

$$H_p(s) = \frac{\rho_w C_{pw}(1 + D_{TI})V_{pf}(T_J - T_I)}{s^2} \times \left\{\exp\left[-\left(\psi\sqrt{\frac{s}{\vartheta}}\tanh\left(\sqrt{\frac{s}{\vartheta}}\right) + s\right)\right] + \frac{T_I}{(T_J - T_I)}\right\} \tag{32}$$

4.2.2. Enthalpy recovery

The energy recovered from the reservoir over a period of time t' can be calculated from following equation:

$$E_p = \int_0^{t'} \dot{m}_w C_{pw}(T_w - T_J)\,dt \tag{33}$$

In terms of the Laplace solution in Eq. (33), the cumulative heat recovery is:

$$E_{\mathrm{p}}(s)=\frac{\rho_{\mathrm{w}}C_{p\mathrm{w}}(1+D_{\mathrm{T1}})V_{\mathrm{pf}}(T_{\mathrm{I}}-T_{\mathrm{J}})}{s^2}\times\left\{1-\exp\left[-\left(\psi\sqrt{\frac{s}{\vartheta}}\tanh\left(\sqrt{\frac{s}{\vartheta}}\right)+s\right)\right]\right\} \quad (34)$$

Selecting the injection temperature as the reference temperature for calculating the initial energy in the geothermal reservoir, the initial amount of heat in the reservoir can be calculated as:

$$E_{\mathrm{R}}=\rho_{\mathrm{r}}C_{p\mathrm{r}}LH[D+(1-\phi)b](T_{\mathrm{I}}-T_{\mathrm{J}}) \quad (35)$$

The thermal recovery efficiency of a geothermal reservoir is defined as the ratio of the amount of energy extracted by the fluid to the initial energy content in the reservoir

$$R(t)=\frac{E_{\mathrm{P}}(t)}{E_{\mathrm{R}}} \quad (36)$$

From Eq. (36), the thermal recovery efficiency in Laplace space is as follows:

$$\Re(s)=\frac{\rho_{\mathrm{w}}C_{p\mathrm{w}}(1+D_{\mathrm{T1}})V_{\mathrm{pf}}}{\lambda LH[D+(1-\phi)b]}\times\frac{1}{s^2}\left\{1-\exp\left[-\left(\psi\sqrt{\frac{s}{\vartheta}}\tanh\left(\sqrt{\frac{s}{\vartheta}}\right)+s\right)\right]\right\} \quad (37)$$

In most cases, $D\gg(1-\phi)b$ and $V_{\mathrm{pf}}=bHL\phi$, and so Eq. (37) can be simplified as follows:

$$\Re(s)=\frac{\rho_{\mathrm{w}}C_{p\mathrm{w}}(1+D_{\mathrm{T1}})b}{\lambda D}\times\frac{1}{s^2}\left\{1-\exp\left[-\left(\psi\sqrt{\frac{s}{\vartheta}}\tanh\left(\sqrt{\frac{s}{\vartheta}}\right)+s\right)\right]\right\} \quad (38)$$

Since it is difficult to invert analytically from the Laplace domain to time domain, the Stehfest algorithm [18] has been implemented. The semi-analytical model thus gives solution for temperature distribution in the fracture and the matrix for the two-phase flow condition. Using this model, the enthalpy production and thermal recovery for different injection and production scenarios can be calculated accurately. Sensitivity studies can be performed by varying reservoir and fracture parameters.

4.3. Extension to fracture network

The results derived for a single fracture have been extended to a fracture network. In order to derive these results, a few additional assumptions have been made in addition to the general assumptions for the single fracture model. These are:

(1) All fractures are vertical with equal lengths and widths.
(2) Permeability and porosity are constant for a given fracture but variable among fractures.
(3) Fluid velocities are proportional only to the ratio of permeability and porosity of the fractures.
(4) Symmetry elements (D for each fracture) are proportional to the relative fluid velocity in adjacent fractures.

The enthalpy production from the fracture network is the summation of enthalpy production individual fractures making up the network.

$$H_{\mathrm{p}}=\sum_{i=1}^{N}H_{\mathrm{p}i} \quad (39)$$

where N is the total number of fractures. To solve the enthalpy production rate from each individual fractures using the single fracture solution, we need to know the symmetry elements, number of fractures, fluid velocities in each fractures Using tracer data we can estimate these parameters and the approaches have been discussed in tracer analysis section. As we discussed in previous section, the required parameters such as mass flow rate in multiple vertical fractures can be estimated from $\frac{\partial F}{\partial \Phi}$ vs. Φ curve using tracer data.

The model and semi-analytic solution developed above is still very useful for fracture characterization and prediction of enthalpy production from real geothermal reservoir with complicated fracture networks despite the assumptions employed in the derivation. In many cases, fractures in naturally or induced superheated geothermal reservoirs are vertical, planar features. Fracture permeability usually varies with fracture aperture and the porosity of the fracture is usually large and close to one. Tortuosity of fracture length (at least to a limited extent) does not alter the predicted enthalpy production dramatically. Furthermore, many assumptions such as constant thermal properties of rock and vapor can be relaxed under geothermal reservoir conditions. The analysis of tracer data can give unique information such as flow/storage capacities of reservoir which can not be obtained otherwise.

5. Application of the algorithms to synthetic models

To validate the models of enthalpy production and thermal recovery from the single fracture model and the fracture network model, the semi-analytical solution is compared with numerical simulation results obtained using TETRAD [19] on some synthetic models. Wu et al. [11,20] have shown the comparison results on swept pore volume estimation, thermal breakthrough time, and enthalpy production rate for single fracture model with superheated initial superheated conditions. Applications of algorithm to geothermal reservoir network as shown in Fig. 4 also have been done and validated using TETRAD numerical simulations, and same conclusions are drawn as shown below. Here we only use a synthetic model with two vertical fractures to demonstrate that the algorithm of calculating enthalpy production from tracer test data is accurate,

Table 1
Summary input data for the conceptual single vertical fracture model

Property	Symbol	Value
Distance between wells (m)	H	200
Length (m)	L	100
Fracture spacing (m)	$2D$	41.06
Half fracture aperture of fracture 1 (m)	$b1$	0.025
Half fracture aperture of fracture 2 (m)	$b2$	0.05
Porosity of fracture 1 (fr)	ϕ_{f1}	0.4
Porosity of fracture 2 (fr)	ϕ_{f2}	0.4
Permeability of fracture 1 (m^2)	$k1$	1×10^{-12}
Permeability of fracture 2 (m^2)	$k2$	5×10^{-13}
Initial reservoir pressure (Pa)	P	3.38×10^7
Initial reservoir temperature (°C)	T_I	240
Initial liquid water saturation	S_{wi}	0.0001
Rock density (kg/m^3)	ρ_r	2650
Rock heat capacity (kJ/kg °C)	C_{pr}	1
Rock thermal conductivity (kJ/m °C s)	λ	0.002884
Injection rate (kg/s)	q	0.133
Producer bottom hole pressure (Pa)	P_{wf}	2.5×10^7
Injection temperature (°C)	T_J	35

and Table 1 summarizes the input data for a simulation with two vertical fractures as depicted in Fig. 6. Initially the reservoir is at saturated conditions with an initial temperature of 240 °C. Cold water is injected at the bottom of the reservoir. A generic tracer with K value of 4500 under reservoir condition is used to represent a highly volatile tracer. The tracer is injected at the very beginning for a period of 0.5 days, and liquid water is continuously injected till the end of simulation. Fig. 8 shows the tracer concentration data in the vapor phase recorded at the producer. The following calculations are made to estimate fracture properties and enthalpy production.

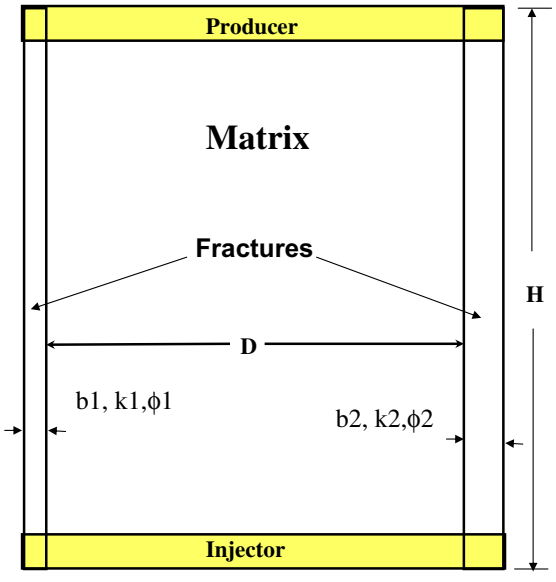

Fig. 6. Diagram of an element of fracture network.

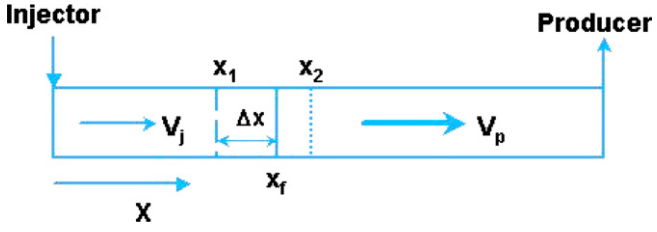

Fig. 7. Two-phase flow in a fracture with phase transition.

From the input data and the reference model we calculate the pore volume of the first fracture as 200 m^3 and the pore volume of the fracture 2 as 400 m^3. The analysis of tracer return curve calculated from TETRAD numerical simulation using Eq. (1) gives the total swept pore volume of 607 m^3, and so the estimation error for total swept pore volume is about 1.2%.

$\frac{\partial F}{\partial \Phi}$ vs. Φ for this problem is plotted in Fig. 9. From this figure we obtain an average normalized interstitial velocities for each fracture as 1.5 for fracture 1 and 0.75 for fracture 2. The fractures are distinguished on the plot by the near-vertical slope at $F = 0.33$; thus, one-third of the total swept pore volume is in fracture 1, and the balance in fracture 2. Using Eq. (6), the ratio of mass flow rates, MR, is 0.5, thus matrix temperature is affected equally by both fractures (this is, D is the fracture half-spacing).

The calculated mass flow rates are used within the semi-analytical formulation to calculate the enthalpy production rate. Fig. 10 compares the energy production rate calculated from the semi-analytical model and that from numerical simulator at early time. In the early time, a few days time lag in predicting liquid breakthrough can be observed; however, given that the high enthalpy production rate endures several decades as seen in Fig. 11 the effect of this initial mismatch is minimal. Furthermore, at early times the enthalpy production rate is relatively low because the mass production rate of vapor is about 10 times smaller than that of liquid water, and this leads to a jump in the enthalpy production rate after 30 days. From Fig. 10 we can see that both the enthalpy production rate and the liquid breakthrough time agree with numerical simulation results. Considering that the semi-analytical solution is unaffected by numerical dispersion, it can be concluded that the semi-analytical model gives a very good estimation of enthalpy production. Differences in the two solutions can be attributed to the following concerns:

- Numerical dispersion in the numerical model. The energy balance calculation uses a single point upstream method, which tends to smear otherwise sharp fronts.
- Non-linear vaporization at the boiling interface. In the analytical derivation, vaporization is assumed to be a linear function of the initial reservoir temperature in the fracture only. This can lead to deviation from numerical modeling.
- The analytic solution assumes constant thermodynamic properties of the fluids, which cannot be mimicked in the model (which uses the correct thermodynamic properties of water).

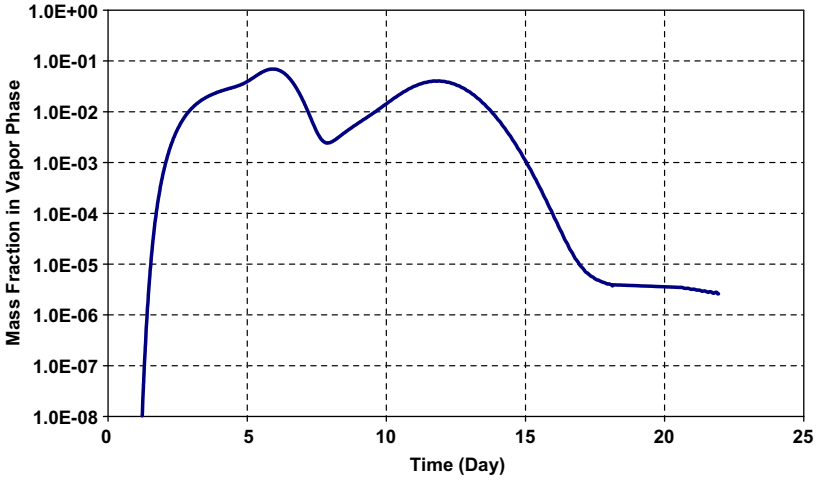

Fig. 8. Tracer concentration in the vapor phase for the two vertical fracture geothermal reservoir. Tracer breaks through the fracture with high permeability, which forms the first "hump" in the figure, and then an abrupt drop before tracer breakthrough at the second fracture with low permeability.

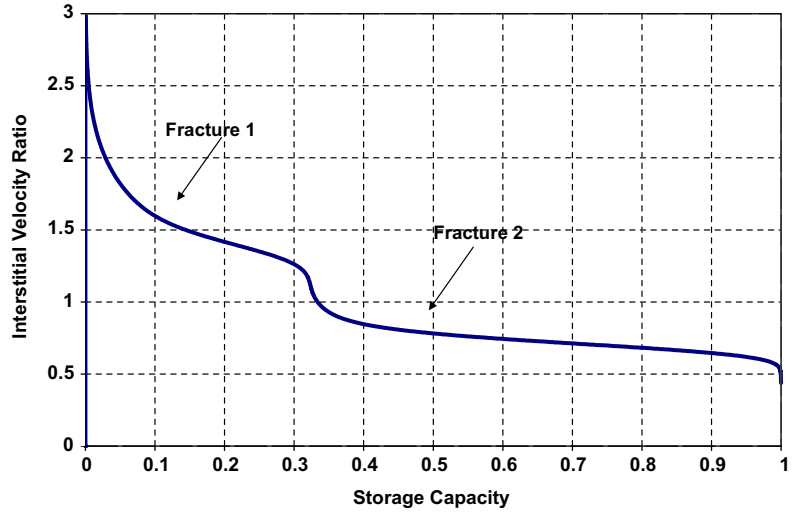

Fig. 9. Interstitial velocity ratio and reservoir storage capacity for the two vertical fracture model. An average value is picked in each segment to calculate the mass flow rate through individual fractures.

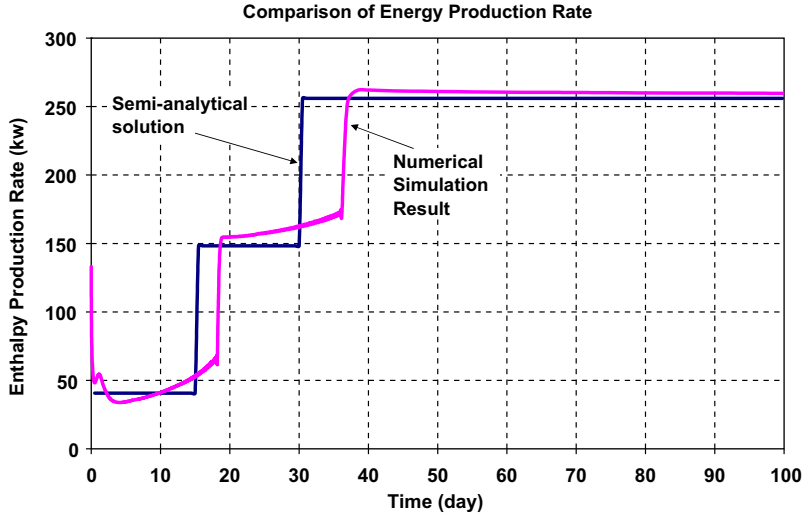

Fig. 10. Early time comparison of enthalpy production between the semi-analytical model and numerical simulation results from TETRAD. The first jump indicates that liquid breakthrough through the fracture with high permeability, while the second one indicates liquid production from both fractures.

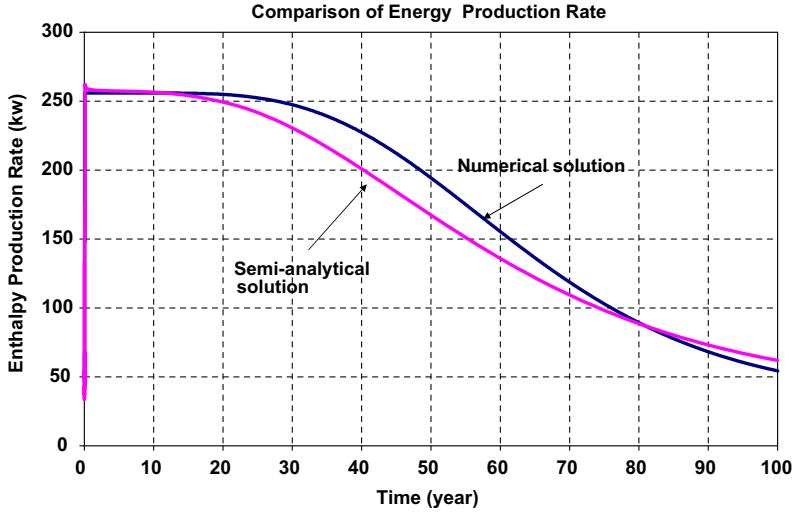

Fig. 11. Comparison of enthalpy production using semi-analytical model with parameters estimated from tracer data and numerical simulation results from TETRAD.

- The liquid/vapor interface was assumed sharp in the analytic model, but was observed to be slightly more diffuse in the numerical model (1–3 grid blocks in length).
- Thermal conduction perpendicular to flow was neglected in the analytic solution, but is isotropic in the numerical model. This is thought to be a weak contributor to the differences noted above.

6. Summary and conclusions

A semi-analytical model for the single fracture model is developed and extended to geothermal reservoirs with a vertical fracture network. Analysis of tracer data yields fracture properties that are subsequently used in the semi-analytical model to calculate the enthalpy production and thermal recovery efficiency. The whole procedure is remarkably simple, robust, and easy to apply to geothermal reservoirs under the special conditions described in this paper.

1. The pore volume of the fracture can be estimated from tracer data using the method of moments for a matrix with either zero or very low permeability.
2. A new solution to the coupled mass and energy flow in a fracture with heat conduction from the matrix has been derived. This new solution is more general than the solution in the literature because it is for a finite matrix rather than a semi-infinite matrix and because it accounts for two-phase flow in the fracture.
3. The distribution of mass rate between the fractures making up the network can be estimated by using the flow capacity versus storage capacity curves. These plots are calculated by computing moments of the tracer return curve.
4. The semi-analytical solution is remarkably simple and fast, so sensitivity studies are readily done and important parameter groupings can be readily identified. The calculated enthalpy production, temperature distribution, and thermal recovery are very close to numerical simulation results from TETRAD.
5. The single fractured geothermal model is extended to the fracture network with different fracture properties. The number of fractures and fractured properties required for energy production can be estimated from tracer information. The algorithm works very well even with high permeability contrast of fractures (20 or higher).

Acknowledgements

This work was funded by the US Department of Energy, Office of Energy Efficiency and Renewable Energy, Geothermal Technology Division, under contract DOE-AC07-05ID14517, whose funding is gratefully acknowledged.

Appendix. Solution of thermal equations for the fracture and the matrix

The governing equations in the matrix and the fracture can be written in dimensionless forms as follows:

$$\frac{\partial T_{\mathrm{Dm}}}{\partial t_{\mathrm{D}}} = \vartheta \frac{\partial^2 T_{\mathrm{Dm}}}{\partial X^2} \tag{A.1}$$

$$\frac{\partial T_{\mathrm{D}}}{\partial t_{\mathrm{D}}} + \frac{\partial T_{\mathrm{D}}}{\partial Z_{\mathrm{D}}} - \psi \left.\frac{\partial T_{\mathrm{Dm}}}{\partial X_{\mathrm{D}}}\right|_{X_{\mathrm{D}}=0} = 0 \tag{A.2}$$

and the initial and boundary conditions are:

$$T_{\mathrm{D}}(X_{\mathrm{D}}, 0) = T_{\mathrm{Dr}}(X_{\mathrm{D}}, Z_{\mathrm{D}}, 0) = 0 \tag{A.3}$$

$$T_{fl}(0, t_{\mathrm{D}}) = 1 \quad \text{for } t_{\mathrm{D}} \geqslant 0 \tag{A.4}$$

$$T_{\mathrm{D}}(Z_{\mathrm{D}}, t_{\mathrm{D}}) = T_{\mathrm{Dr}}(Z_{\mathrm{D}}, 0, t_{\mathrm{D}}); \tag{A.5}$$

$$\left.\frac{\partial T_{\mathrm{Dr}}}{\partial X_{\mathrm{D}}}\right|_{X_{\mathrm{D}}=1} = 0 \tag{A.6}$$

Applying Laplace transformation method with respect to t_D to Eqs. (A.1) and (A.2), we can get:

$$\frac{\partial^2 \upsilon}{\partial X_D^2} - \frac{s}{\vartheta}\upsilon + \frac{1}{\vartheta}\upsilon(0) = 0 \tag{A.7}$$

$$s\eta - \eta(0) + \frac{\partial \eta}{\partial Z_D} - \psi \left.\frac{\partial \upsilon}{\partial X_D}\right|_{X_D=0} = 0 \tag{A.8}$$

where u and v are temperature of the fracture and matrix in the Laplace space, respectively. The boundary conditions of Eqs. (A.4)–(A.6) in Laplace domain are:

$$\eta(0) = \frac{1}{s} \tag{A.9}$$

$$\eta(z_D) = \upsilon(z_D, 0) \tag{A.10}$$

$$\left.\frac{\partial \upsilon}{\partial x_D}\right|_{X_D=1} = 0 \tag{A.11}$$

Applying initial conditions in Laplace space, $v(0) = 0$ and $u(0) = 0$, we have following equations:

$$\begin{aligned} &su + \frac{\partial u}{\partial Z_D} - \psi \left.\frac{\partial v}{\partial X_D}\right|_{X_D=0} = 0 \\ &\frac{\partial^2 v}{\partial X_D^2} - \frac{s}{\vartheta} v = 0 \end{aligned} \tag{A.12}$$

Solving the second equation gives:

$$\upsilon = C_1 \cosh\left(\sqrt{\frac{s}{\vartheta}} X_D\right) + C_2 \sinh\left(\sqrt{\frac{s}{\vartheta}} X_D\right) \tag{A.13}$$

where C_1 and C_2 are constants, applying boundary conditions given in Eqs. (A.10) and (A.11), C_1 and C_2 can be determined:

$$C_2 = -C_1 \tanh\left(\sqrt{\frac{s}{\vartheta}}\right) \tag{A.14}$$

$$C_1 = \eta \tag{A.15}$$

Substituting above into Eq. (A.13) gives:

$$\upsilon = \eta\left[\cosh\left(\sqrt{\frac{s}{\vartheta}} X_D\right) - \sinh\left(\sqrt{\frac{s}{\vartheta}} X_D\right) \tanh\left(\sqrt{\frac{s}{\vartheta}}\right)\right] \tag{A.16}$$

Now solve the equation for the temperature in the fracture:

$$\left.\frac{\partial \upsilon}{\partial X_D}\right|_{X_D=0} = -u\sqrt{\frac{s}{\vartheta}} \tanh\left(\sqrt{\frac{s}{\vartheta}}\right) \tag{A.17}$$

Substitution of above equation into fracture equation gives:

$$s\eta + \frac{\partial \eta}{\partial Z_D} + \psi u \sqrt{\frac{s}{\vartheta}} \tanh\left(\sqrt{\frac{s}{\vartheta}}\right) = 0 \tag{A.18}$$

The solution of above equation is:

$$u = C_3 \cdot \exp\left[-\left(\psi\sqrt{\frac{s}{\vartheta}} \tanh\left(\sqrt{\frac{s}{\vartheta}}\right) + s\right) Z_D\right] \tag{A.19}$$

Applying boundary conditions gives to above equations, we have that

$$C_3 = \frac{1}{s} \tag{A.20}$$

and the final solution for above equation is:

$$\eta = \frac{1}{s} \exp\left[-\left(\psi\sqrt{\frac{s}{\vartheta}} \tanh\left(\sqrt{\frac{s}{\vartheta}}\right) + s\right) Z_D\right] \tag{A.21}$$

Substitution of temperature in fracture model to the equation of temperature in matrix, we have the temperature in matrix equation as:

$$\begin{aligned} \upsilon = \frac{1}{s} \exp\left[-\left(\psi\sqrt{\frac{s}{\vartheta}} \tanh\left(\sqrt{\frac{s}{\vartheta}}\right) + s\right) Z_D\right] \Bigg[\cosh\left(\sqrt{\frac{s}{\vartheta}} X_D\right) \\ - \sinh\left(\sqrt{\frac{s}{\vartheta}} X_D\right) \tanh\left(\sqrt{\frac{s}{\vartheta}}\right)\Bigg] \end{aligned} \tag{A.22}$$

Special Case 1: $D \to 0$

When $D \to 0$, we have $\vartheta \to \infty$, and $\tanh\left(\sqrt{\frac{s}{\vartheta}}\right) \to 0$. In this situation, (A.21) is:

$$\begin{aligned} \lim_{\vartheta\to\infty}(\eta) &= \lim_{\vartheta\to\infty}\left\{\frac{1}{s} \exp\left[-\left(\psi\sqrt{\frac{s}{\vartheta}} \tanh\left(\sqrt{\frac{s}{\vartheta}}\right) + s\right) Z_D\right]\right\} \\ &= \frac{1}{s} \exp[-sZ_D] \end{aligned} \tag{A.23}$$

Using Inverse Laplace transform, we can get the dimensionless temperature in the fracture as follows.

$$T_{fD} = \delta(t_D - Z_D) \tag{A.24}$$

Physically t_D means the thermal front location along the fracture at any given time, and $\delta(t_D - Z_D)$ is a Dirac's Delta Function with following property:

$$\delta(t_D - Z_D) = \begin{cases} 1 & t_D \geqslant Z_D \\ 0 & t_D < Z_D \end{cases} \tag{A.25}$$

In other words, in one-dimension flow, the temperature is in a form of sharp wave that changes from the injection temperature to the initial temperature.

Special Case 2: $D \to \infty$

When $D \to \infty$, we have $\vartheta \to 0$, and $\tanh\left(\sqrt{\frac{s}{\vartheta}}\right) \to 1$. In this situation, Eq. (A.21) is:

$$\begin{aligned} \lim_{\vartheta\to\infty}(\eta) &= \lim_{\vartheta\to\infty}\left\{\frac{1}{s} \exp\left[-\left(\psi\sqrt{\frac{s}{\vartheta}} \tanh\left(\sqrt{\frac{s}{\vartheta}}\right) + s\right) Z_D\right]\right\} \\ &= \frac{1}{s} \exp\left[-\left(\psi\sqrt{\frac{s}{\vartheta}} + s\right) Z_D\right] \end{aligned} \tag{A.26}$$

In dimensionless time space, the dimensionless temperature is as follows:

$$T_{fD} = \operatorname{erfc}\left\{\frac{\psi Z_D}{2[\vartheta(t_D - Z_D)]^{1/2}}\right\} \tag{A.27}$$

References

[1] J.W. Lund, The USA geothermal country update, Geothermics 32 (2003) 409–418.

[2] G.S. Bodvasson, Thermal problems in sitting of reinjection wells, Geothermics 1 (2) (1972) 63–66.

[3] G.M. Shook, Predicting thermal breakthrough in heterogeneous media from tracer tests, Geothermics 30 (6) (2001) 573–589.

[4] H.A. Lauwerier, The transport of heat in an oil layer caused by the injection of hot fluid, Appl. Sci. Res. 5 (2–3) (1955) 145–150.

[5] K. Pruess, G.S. Bodvarsson, Thermal effects of reinjection in geothermal reservoirs with major vertical fractures, J. Petrol. Technol. 36 (1984) 1567–1578.

[6] I. Kocabas, Geothermal reservoir characterization via thermal injection backflow and interwell tracer testing, Geothermics 34 (1) (2004) 27–46.

[7] H.S. Carslaw, J.C. Jaeger, Conduction of Heat in Solids, second ed., Oxford Science Publications, 1959, p. 396.

[8] G.S. Bodvarsson, C.F. Tsang, Injection and thermal breakthrough in fractured reservoirs, J. Geophys. Res. 87 (B2) (1982) 1031–1048.

[9] S. Finsterle, P. Persoff, Determining permeability of tight rock samples using inverse modeling, Water Resour. Res. 33 (8) (1997) 1803–1812.

[10] W.R. Rossen, Y. Gu, L.W. Lake, Connectivity and permeability in fracture networks obeying power-law statistics, SPE59720, in: Proceedings of the 2000 Permian Basin Oil and Gas Recovery Conference, Midland, TX, March 21–23, 2000.

[11] X. Wu, G.A. Pope, G.M. Shook, S. Srinivasan, A method of analyzing tracer data to calculate swept pore volume in fractured geothermal reservoirs under two-phase flow conditions, in: Proceedings of 30th Workshop on Geothermal Reservoir Engineering, Stanford, CA, January 31–February 2, 2005.

[12] V. Dwarakanath, N. Deeds, G.A. Pope, Analysis of partitioning interwell tracer tests, Environ. Sci. Technol. 33 (1999) 3829–3836.

[13] R. Sinha, K. Asakawa, G.A. Pope, K. Sepehrnoori, Simulation of natural and partitioning interwell tracers to calculate saturation and swept volumes in oil reservoirs, SPE 89458, in: Proceedings of the 2004 SPE/DOE Fourteenth Symposium on Improved Oil Recovery, Tulsa, OK, April 17–21, 2004.

[14] X. Wu, An investigation of partitioning tracers for characterizing geothermal reservoirs and predicting enthalpy production, Ph.D. dissertation, The University of Texas at Austin, Austin, TX, 2006.

[15] V. Dwarakanath, N. Deeds, G.A. Pope, Analysis of partitioning interwell tracer tests, Environ. Sci. Technol. 33 (1999) 3829–3836.

[16] L.W. Lake, Enhanced Oil Recovery, Prentice-Hall, New Jersey, 1989, pp.195–196.

[17] G.M. Shook, A simple, fast method of estimating fractured geometry from tracer tests, Geothermal Resour. Council Trans. 27 (2003).

[18] H. Stehfest, Numerical inversion of Laplace transform, Commun. ACM 13 (1979) 44–49.

[19] P.K.W. Visome, G.M. Shook, Multipurpose simulation, J. Petrol. Eng. 9 (1993) 29–38.

[20] X. Wu, G.A. Pope, G.M. Shook, S. Srinivasan, A semi-analytical model to calculate energy production in the single fracture geothermal reservoirs, Geothermal Resour. Council Trans. 29 (2005) 665–669.